



Three-dimensional imaging through patterned type-1 microscopy

G. SAAVEDRA, A. GIMENO-GÓMEZ, M. MARTÍNEZ-CORRAL,*  J. SOLA, AND E. SÁNCHEZ-ORTIGA 

3D Imaging and Display Laboratory. Department of Optics, University of Valencia, E46100 Burjassot, Spain

**manuel.martinez@uv.es*

Abstract: We report a scanning non-confocal fluorescence microscopy scheme that provides images with optical sectioning and with a lateral resolution that surpasses by a factor of two the diffraction resolution limit. This technique is based on the type-1 microscopy concept combined with patterned illumination. The method does not require the application of phase-shifting or post-processing algorithms and provides artifact-free superresolved 3D images. We have validated the theory by means of experimental data.

© 2021 Optica Publishing Group under the terms of the [Optica Open Access Publishing Agreement](#)

1. Introduction

In a seminal contribution Wilson and Sheppard [1] presented the concepts of type-1 and type-2 scanning microscopy and compared them with the conventional widefield (WF) microscope. In a type-1 scheme the object is illuminated uniformly and a point detector is scanned across the image space. The type-1 arrangement has imaging properties identical to a WF microscope. On the contrary, in the type-2 scheme a point source illuminates a very small region of the object, and a point detector collects light only from that region. An image is built up by scanning the source and detector in synchronism. This later arrangement corresponds to confocal scanning microscopes (CSM).

The main feature of CSMs is that, as compared with WF ones, they enhance 3D resolution; that is, they provide images with extended cut-off frequency along both the lateral and the axial directions. In particular, systems able to extend the axial cut-off frequency are said to have optical sectioning capability. This capability has encouraged research in scanning microscopy. In this context, it is remarkable Stimulated Emission Depletion (STED) [2], microscopic imaging with minimum photon fluxes (MINFLUX) [3], and variations of the confocal concept [4–14], which benefit from the multiplicative nature of their point spread function (PSF). An advantage of scanning microscopes is that they are straightforward in terms of the computational effort needed for retrieving the high-resolution components. However, the need for focused-beam illumination slows the process and increases the photodamage. Among those microscopes, recently has attracted great interest the proposal of combining the image scanning concept [9] with multifocal illumination [10,11]. This architecture is fully based on confocal concept and has the advantage of providing confocal resolution and optical sectioning but with faster acquisition speed. Also interesting is the approach reported in [12] which, based in the confocal concept, takes profit from the pixel offset [14], the image scanning concept and the Fourier filtering.

Non-scanning techniques under extended illumination have been reported as well. This is the case of Structured-Illumination Microscopy (SIM) [15–25], in which a periodic illumination beam is projected onto the sample. In SIM the information contained in the final image is extended, so that it includes details of the sample with spatial frequency higher than the cut-off frequency of a WF microscope. However, specific time-costly reconstruction algorithms, including image-processing procedures, are required in order to retrieve the high-resolution

information. To avoid the computer artifacts, a realization of SIM with two-photon fluorescence was proposed [26]. The light efficiency of this approach is much poorer.

In this paper we report a microscope scheme with the ability of providing 3D resolution but overcoming above drawbacks. The scheme is based on the type-1 concept, but with patterned illumination. We have named the technique as Type-1 Patterned-Illumination Microscopy (T1PIM). The T1PIM provides images with lateral resolution that doubles the diffraction limit and with an optical-sectioning capability similar to that of confocal microscopes. Besides, it does not require for the use of phase-shifting or for image post-processing. Thus, it is free from the artifacts that can appear in SIM. Although we are aware of the importance of postprocessing tools, it is clear that the primary important issue is the information captured by the system. Naturally, there is still much room for computer-processing improvements. It is worth noting here that the T1PIM is different both conceptually and experimentally from multifocal SIM [10,11], which uses for illumination an array of focused spots and is based on the type-2 concept. From an optical point of view, multifocal SIM provides the same resolution and optical sectioning as confocal, but with faster acquisition speed.

2. Type-1 patterned-illumination microscope

To demonstrate our claims, we start by considering a fluorescence WF microscope in which a 3D sample with a distribution of fluorophores $O(\mathbf{r})$ is placed at the object plane and is illuminated by a light beam with intensity structure, $S(\mathbf{r})$. Assuming telecentricity, the 3D intensity distribution in the image space is calculated, through a 3D convolution, as

$$I_{3D}(\mathbf{r}) = [O(\mathbf{r}) S(\mathbf{r})] \otimes h(\mathbf{r}) \quad (1)$$

where $\mathbf{r} = (x, z)$ stand for the normalized spatial coordinates, as defined in [5], and $h(\mathbf{r})$ for the 3D intensity PSF.

Next, we analyze the systems which we name here as pinholed-collection scanning (PS) microscopes, in which only the light passing through a pinhole is collected. In these microscopes a 2D scanning is required for capturing any depth section of the image. For capturing the 3D image, the sample is axially scanned as well. For each scanning position of the sample, \mathbf{r}_s , the intensity of light emitted by a small region of the object is integrated. Mathematically,

$$I_{PS}(\mathbf{r}_s) = \int d^3\mathbf{r} [O(\mathbf{r} + \mathbf{r}_s) S(\mathbf{r})] \otimes h(\mathbf{r}) \delta(\mathbf{r}) \quad (2)$$

where the Dirac delta function, $\delta(\mathbf{r})$, accounts for the role of the pinhole. Assuming that the illumination pattern is fully symmetric, $S(x, y, z) = S(-x - y, z)$, we can rewrite Eq. (2) as

$$I_{PS}(\mathbf{r}_s) = O(\mathbf{r}_s) \otimes_3 [S(\mathbf{r}_s) h(\mathbf{r}_s)] \quad (3)$$

When comparing Eqs. (1) and (3) one realizes the main advantage of PS microscopes over WF ones: function S moves from multiplying at O to multiplying at h . Then, a new 3D PSF, $S(\mathbf{r}_s) h(\mathbf{r}_s)$, is obtained. This property can be understood, as well, in the Fourier domain,

$$\tilde{I}_{PS}(\mathbf{k}) = \tilde{O}(\mathbf{k}) [\tilde{S}(\mathbf{k}) \otimes_3 H(\mathbf{k})] \quad (4)$$

where the symbol \sim stands for Fourier transformed, \mathbf{k} for the normalized spatial-frequency coordinate, and H for the 3D optical transfer function (OTF) of the WF microscope. The term between brackets, $\tilde{S}(\mathbf{k}) \otimes H(\mathbf{k})$, represents the OTF of the PS microscope.

The WF microscope can be considered as the limit of PS microscopes provided that $S(\mathbf{r}) = 1$, or equivalently $\tilde{S}(\mathbf{k}) = \delta(\mathbf{k})$. Then

$$I_{WF}(\mathbf{r}_s) = O(\mathbf{r}_s) \otimes_3 h(\mathbf{r}_s) \tag{5}$$

Other case is the CSM in which $S(\mathbf{r}) = h(\mathbf{r})$, or equivalently $\tilde{S}(\mathbf{k}) = H(\mathbf{k})$. Then

$$I_{CSM}(\mathbf{r}_s) = O(\mathbf{r}_s) \otimes_3 h^2(\mathbf{r}_s) \tag{6}$$

In Fig. 1 we show the PSF and the OTF of WF and confocal microscopes. Assuming the ideal case of infinitesimal pinhole, the lateral resolution of CSMs is clearly superior to that of WF ones. However, in case of realistic pinhole sizes, such resolution improvement diminishes [27]. Note however that the main advantage of CSMs over WF ones is not the gain in lateral resolution, but the optical sectioning capability, which we will study later. Furthermore, other schemes based on confocal concept show a similar behavior [13].

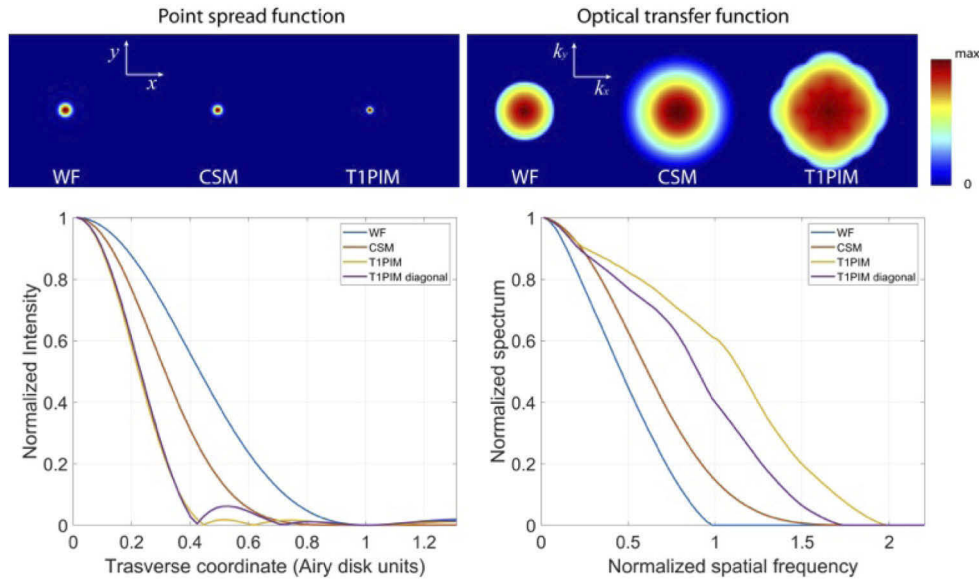


Fig. 1. 2D PSF and OTF for WF, CSM, and T1PIM.

Aiming to improve the lateral resolution and obtaining optical sectioning capability, we propose here the T1PIM by using a laterally periodic illumination. Being $S(\mathbf{r})$ periodic, $\tilde{S}(\mathbf{k})$ comprises some equidistant delta functions. As result, a widening in the OTF, and therefore a narrowing in the PSF, is achieved.

To make more comprehensible the proposal, we consider the illumination pattern resulting from the interference of four coherent plane waves travelling with symmetric angles with respect to the optical axis. In amplitude the illumination spectrum consists of four deltas placed at the corners of a square circumscribed in the circle defined by the aperture stop. This arrangement of planes waves, produces an illumination pattern that is periodic along (x, y) , but constant along the axial direction. In consequence, we can simplify the mathematics by dismissing the z component in the illumination function

$$S(x, y) = |e^{j\pi Ax} + e^{-j\pi Ax} + e^{j\pi Ay} + e^{-j\pi Ay}|^2 = 4|\cos(\pi Ax) + \cos(\pi Ay)|^2 \tag{7}$$

where A is a spatial-frequency constant related with the angular inclination of the plane waves. Expressed in the frequency domain, this formula reads

$$\begin{aligned} \tilde{S}(k_x, k_y) = & 4\delta(k_x, k_y) + \delta(k_x - A, k_y) + \delta(k_x + A, k_y) + \delta(k_x, k_y - A) + \delta(k_x, k_y + A) + \\ & + 2 \left[\delta \left(k_x - \frac{A}{2}, k_y - \frac{A}{2} \right) + \delta \left(k_x + \frac{A}{2}, k_y + \frac{A}{2} \right) + \delta \left(k_x - \frac{A}{2}, k_y + \frac{A}{2} \right) + \delta \left(k_x + \frac{A}{2}, k_y - \frac{A}{2} \right) \right] \end{aligned} \quad (8)$$

Then, the extended lateral OTF

$$H_{\text{T1PIM}}(k_x, k_y) = \tilde{S}(k_x, k_y) \otimes H(k_x, k_y) \quad (9)$$

is formed by the superposition of nine, shifted, widefield OTFs.

To illustrate this fact, we obtained the direct image of a fluorescent USAF 1951 test target illuminated with the periodic pattern, see Fig. 2(a). In Fig. 2(b) we show the Fourier transform of the image. The 9 different spectral components, that include high-resolution information of the object spectrum, are clearly seen.

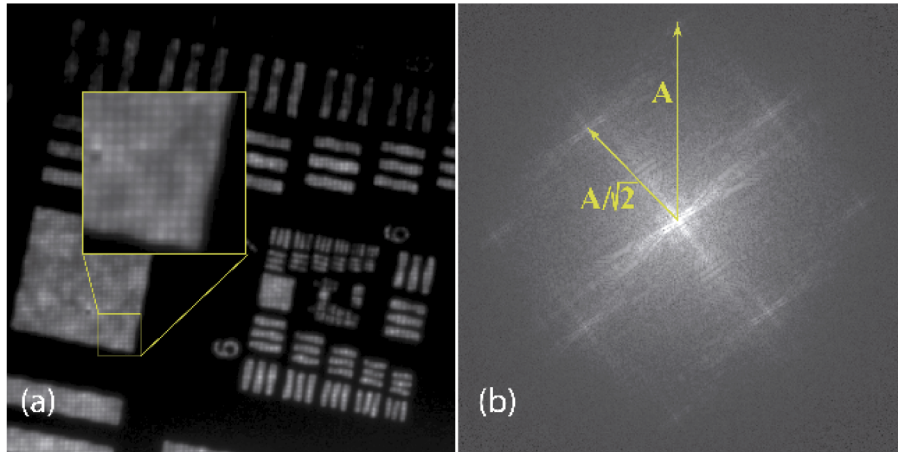


Fig. 2. Intensity distribution in the camera plane resulting from the interaction between the sample and the illumination; (b) its Fourier transform

If we compare the T1PIM with the previously described systems, we find that while in WF $\tilde{S}(\mathbf{k})$ is confined to one delta, and in CSM, $\tilde{S}(\mathbf{k})$ is a continuous and compact-support function; in T1PIM the $\tilde{S}(\mathbf{k})$ is confined to a set of equidistant deltas. For the three cases, the result of the convolution between $\tilde{S}(\mathbf{k})$ and $H(\mathbf{k})$ are shown in Fig. 1(b)). Clearly, the width of resulting OTF is much wider in the T1PIM case. Explained in other words, as result of the patterned illumination, the pinhole collects the information of its object conjugate as illuminated by four plain waves. Then, after the scanning the final intensity image has collected a much broader frequency content since its support is the result of composing nine shifted WF supports. On the contrary in, for example, the ideal confocal case, the OTF is the result of the self-correlation of the WF OTF, resulting in an OTF that is twice broader than the WF one, but poorly efficient in the high frequencies.

In Fig. 1 we have shown the H_{T1PIM} and also the $\text{PSF}_{\text{T1PIM}}$. Since these functions are not radially symmetric, we represented the curves for two directions: the k_x and the diagonal one. When evaluating the lateral resolution, it is preferable not to use the value of the cut-off frequency (which does not take into account the efficiency at high frequencies), but the width of the OTF at a 10% of its maximum value. From the curves we obtain the following theoretical values: $\text{WF}=0.81$, $\text{CSM}=1.08$, $\text{T1PIM}_{\text{diag}}=1.42$ and $\text{T1PIM}_x=1.68$. This confirms the superiority, in terms of lateral resolution, of T1PIM.

An essential feature of TIPIM is that the resolution gain is achieved directly without the need of post-processing or additional computation. Naturally, one can apply postprocessing to further improve the image quality.

3. Experimental verification

We have built in the laboratory a TIPIM by adding an illumination arm to a WF microscope (which is named here as the host microscope) see Fig. 3. To create the structured illumination, we have used the combination of two Fresnel biprisms with different birefringence angle (1.0° and 1.5°) and set with their edges perpendicular to each other. Biprisms have been used before for generating conventional structured illumination [28–29], and are especially suitable for our purpose, as most of light coming from the laser source arrives at the sample. The biprisms are placed in front of the output laser light ($\lambda = 488 \text{ nm}$) to generate four mutually coherent virtual point sources in rectangular grid. The distance between the virtual sources depends on the biprism angle and on the distance between the biprisms and the exit of the fiber. By choosing the proper axial gap between the biprisms, the virtual sources can be placed at the vertices of a square. Experimentally, this is made by axially displacing the biprisms at the time that the virtual sources are observed. The combination between the collimating lens, $f_{\text{col}} = 100 \text{ mm}$, and the illumination lens, $f_{\text{ill}} = 300 \text{ mm}$, provides the image of the virtual sources onto the aperture stop of an infinity-corrected microscope objective. Thus, at the object plane an extended patterned illumination is obtained, whose period is inversely proportional to the distance between the virtual sources.

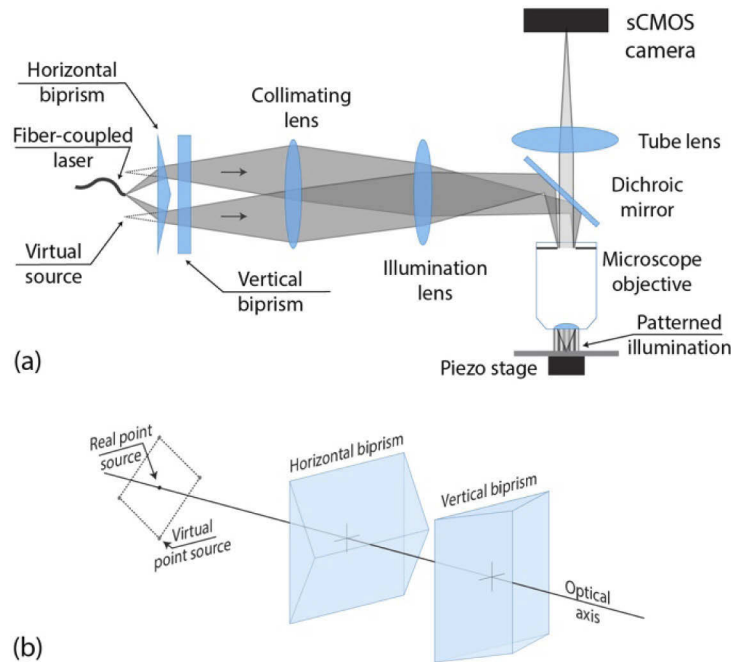


Fig. 3. (a) Scheme of the experimental setup. In the ray tracing we have shown only the action of the horizontal biprism; (b) Enlarged view of biprisms action in the illumination arm.

The light emitted by the sample is collected by the same microscope objective and imaged onto the camera (Quantalux CS2100M sCMOS, with pixel size $\delta_p = 6.6 \mu\text{m}$) by means of a tube

lens of $f_{TL} = 300 \text{ mm}$. This large focal length was chosen for achieving a good sampling of the periodic pattern.

For the scanning, the sample was mounted on a piezo-stage (PI P-611 Nanocube), which permits displacements of $100 \mu\text{m}$ with precision step of 1 nm . We developed a user interface in Labview©, which allowed the selection of some specific pixels of the camera and the integration of their intensity for every scanning step [6–9]. This way of proceeding is equivalent to collect with a large area detector the light passing through a pinhole.

With this set-up we performed first a proof-of-concept experiment for confirming the resolution improvement achieved by T1PIM. We used a fluorescent-dyed USAF test target as sample. The highest spatial frequency of that USAF test (645.1 mm^{-1}) is not high enough to test the resolution of high-NA microscopes. Thus, we performed this experiment with a low-NA objective ($10\times$ NA=0.10). The period of projected illumination pattern was $p = 2.44 \mu\text{m}$, and the pixel size, as evaluated in the object space was $\delta = 0.44 \mu\text{m}$. The radius of the Airy disk at the object space was $\rho = 2.98 \mu\text{m}$.

For obtaining the T1PIM image, we selected within the sCMOS a synthetic pinhole of 2×2 pixels ($13.2 \times 13.2 \mu\text{m}$) and scanned laterally the USAF test. With the same setup, but after removing the biprisms, we captured a second image, which is equivalent to a WF image. The two images are shown in Fig. 4.

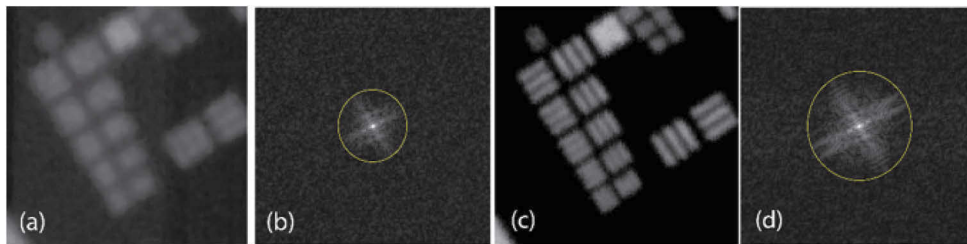


Fig. 4. (a) Image of the USAF test obtained with the WF setup; (b) The Fourier transform of (a); (c) Image of the USAF test obtained with the T1PIM; (d) Fourier transform of (c). In the lateral scanning the step size was of 35 nm and the number of steps 200×200 .

Note that spatial-frequency content of the T1PIM image is much wider than that of the WF image. On the other hand, the last element resolved is the 8.4, which has a linewidth of $1.38 \mu\text{m}$. This value is equal to the resolution provided, ideally, by a WF microscope with NA = 0.18, which almost doubles the used NA.

The second experiment was made to confirm the optical-sectioning capability of T1PIM. Usually, the optical sectioning is checked by measuring the integrated intensity function [1]. This function is defined as the integral over lateral coordinates of the 3D PSF. Experimentally is often evaluated by measuring the response to an axially-scanned fluorescent layer. For that purpose, we embedded a drop of Rhodamine 123 between a slide and a coverslip. Since we had no longer problems with the resolution provided by the USAF, we used a high-NA dry objective ($60\times$ NA=0.6). In this case the period of projected illumination pattern was $p = 0.37 \mu\text{m}$, while the pixel size in the object space was $\delta = 0.073 \mu\text{m}$. The radius of the Airy disk at the object space was $\rho = 0.50 \mu\text{m}$. The (x, z) sections of the resulting 3D images are shown in Fig. 5(a) and (b). From those images we obtained, after integration over (x, y) , the integrated intensities, which are shown in Fig. 5(c). In the WF case the integrated intensity is almost uniform, as expected in systems with no optical sectioning capability. On the contrary, in T1PIM the signal falls quickly when the layer is scanned out from the focal plane. The full width at half maximum (FWHM) of the integrated intensity is the parameter used for determining the axial resolution.

Here, it is around $2.0 \mu\text{m}$, which is quite close to that of a CSM with the same NA (assuming an infinitesimal pinhole, in CSM the theoretical value is $\text{FWHM}=1.7 \mu\text{m}$).

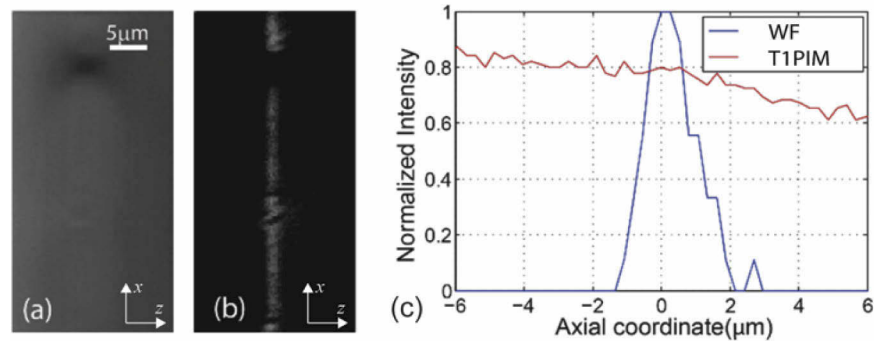


Fig. 5. (x, z) section of the 3D image obtained after scanning axially a thin fluorescent layer, corresponding to: (a) WF microscope and (b) T1PIM. (c) Integrated intensity of both microscopes.

4. Parallelized capture

Perhaps the main drawback of T1PIM as presented above is the large acquisition time, which compromises the temporal resolution. To reduce drastically that time, we take profit of both the periodic structure of the illumination and the pixelated detection, for implementing a parallelized capture. The idea is to record in parallel the intensity of pixels corresponding to the maxima of the illumination pattern. Experimentally, these pixels are determined from a preliminary image obtained in absence of sample. Then, for capturing the T1PIM image, the sample only needs to be scanned laterally a distance equal to the pattern period. Since the distance between consecutive maxima of our illumination pattern is approximately equal to the resolution limit of the host microscope, only 4×4 steps are necessary to meet the Nyquist criterion. However, 6×6 scanning points were chosen to oversample the $\text{PSF}_{\text{T1PIM}}$.

To illustrate the parallelization procedure, we present an example performed with a low-NA (0.1) objective and the fluorescent USAF 1951 test target, see Fig. 6. From the image directly captured by the sensor, a parallelized image can be generated using the fraction of pixels corresponding to the maxima of the illumination pattern. Later, a lateral scanning of the sample permits to capture subregions within those maxima. The number of parallel scanning points depends on the overlapping region of the four plane waves as well as on their interference angle.

We implemented the parallelized acquisition for an Olympus 60x NA=1.25 oil-immersion objective. The performance of the system was evaluated for two different samples: a non-biological and a biological one. Again, the period of projected illumination pattern was $p = 0.37 \mu\text{m}$, and the pixel size in the object space $\delta = 0.073 \mu\text{m}$. The radius of the Airy disk at the object space was $\rho = 0.24 \mu\text{m}$.

To evaluate accurately the lateral resolution, we first obtained a 2D image of a sparse distribution of carbon nanoparticles [30] of 100 nm of mean radius. The field of view covered 110×110 maxima of the structured pattern and the object was scanned in parallel with steps of 42 nm, producing an image of 660×660 pixels. The acquisition time was 1.8 s. A comparison between the conventional and the T1PIM image is shown in Fig. 7. The expected bandwidth extension and shape in the T1PIM is proven by the Fourier transform of the acquired image.

To quantify the improvement in lateral resolution, we computed a profile along the center of one of the carbon nanoparticles present in the image, see Fig. 8 (left). From the graph, we found almost twofold improvement in lateral resolution: $\text{FWHM}_{\text{WF}} = 230 \text{ nm}$ and $\text{FWHM}_{\text{T1PIM}} = 120 \text{ nm}$.

We computed also a profile of the Fourier transform. Aiming to reduce the noise, we first computed the 1D FT along 500 rows of the image. Then we averaged the 500 1D FTs. The final profiles are shown in Fig. 8 (right). This confirms that the OTF at 10% of T1PIM doubles that of WF microscope.

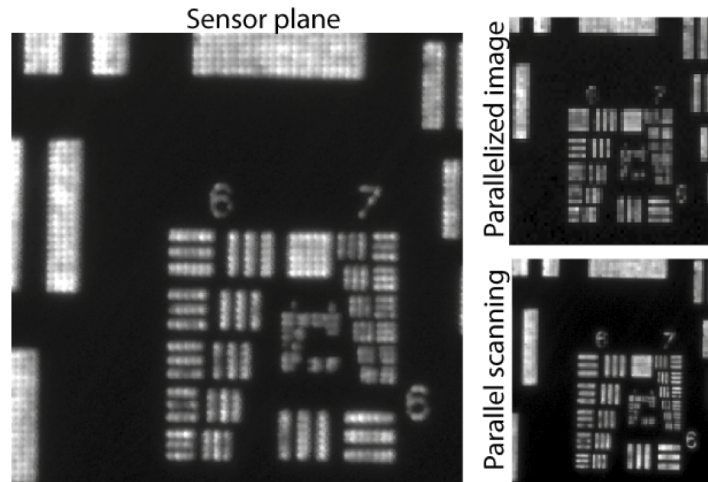


Fig. 6. Example of a parallel acquisition with the proposed system. Each position corresponding to a maximum of the structured pattern is detected as a pixel of the parallelized image. To produce the high-resolution parallel scanning image, the sample is laterally scanned in a subregion within two maxima.

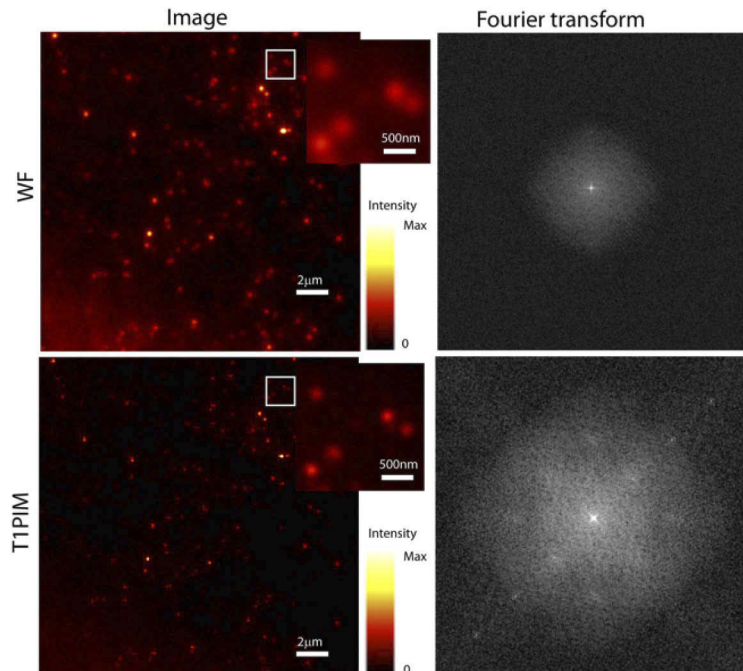


Fig. 7. Comparison of the images of carbon nanoparticles (left) and their corresponding Fourier transforms (right) for WF microscopy and T1PIM.

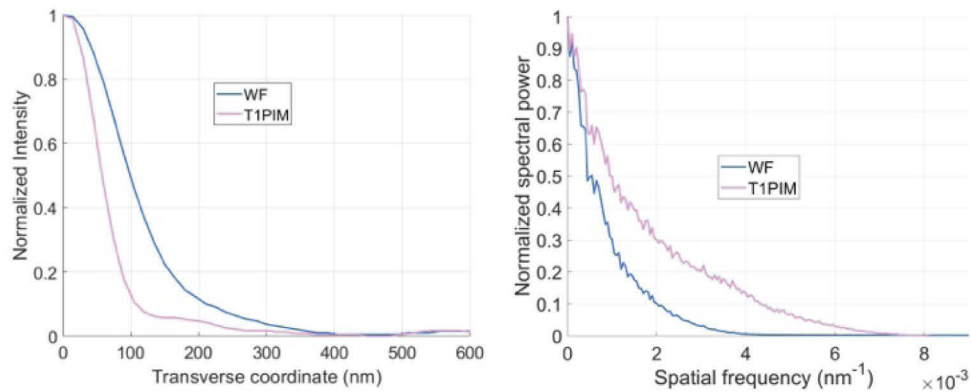


Fig. 8. (Left) Profiles of the 2D PSF measured from the image of a carbon nanoparticle for conventional WF microscopy and for T1PIM. (Right) Averaged OTF computed from a set of OTF profiles for conventional WF microscopy and T1PIM.

To confirm the utility of our method with biological samples, we obtained with the same setup the image of F-actin of muntjac skin fibroblasts (Alexa Fluor 488) from Fluocells prepared slide #6, see Fig. 9.

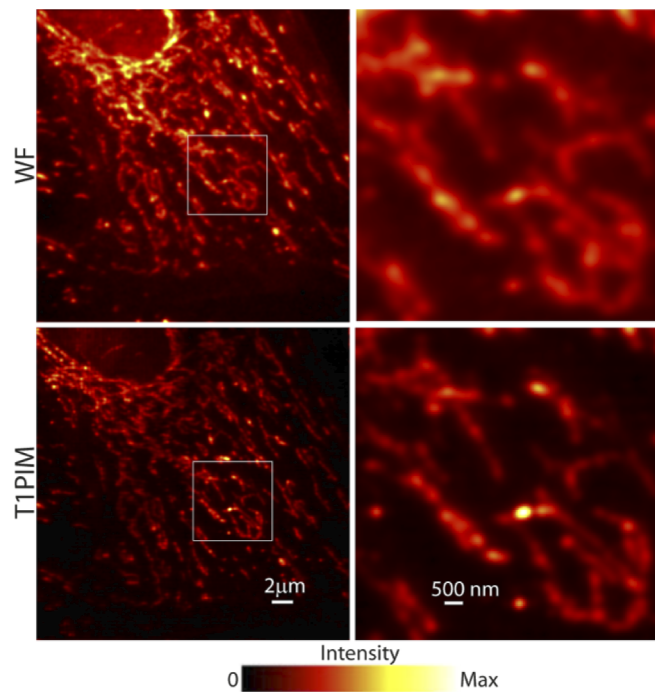


Fig. 9. Images of actin from muntjac cells captured by conventional WF microscopy (top) and by T1PIM (bottom). In the right column we show enlarged views of the insets.

Aiming to show the optical sectioning capability of T1PIM, a z-stack of the muntjac cells was captured for both the conventional microscope and the T1PIM. In Fig. 10 two renders of the maximum intensity projection volumes produced by the z-stacks are shown. This illustrates that T1PIM provides both the expected lateral improvement and the optical sectioning.

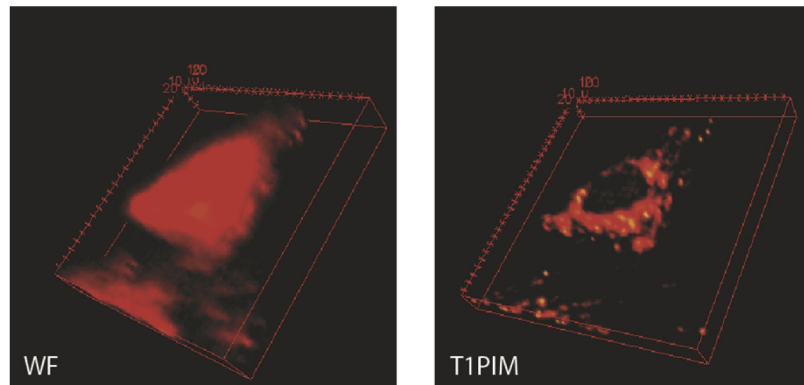


Fig. 10. A frame of the 3D render of a z-stack of muntjac cells obtained with WF microscopy and with T1PIM. The movie from which the frame has been extracted is in [Visualization 1](#).

Finally, in Fig. 11 we show meridional cuts along (k_x, k_z) of the 3D Fourier transform of the z-stacks. The filling of the missing cone of captured frequencies, which demonstrates the optical sectioning capability, and the extension of lateral cut-off frequency are apparent.

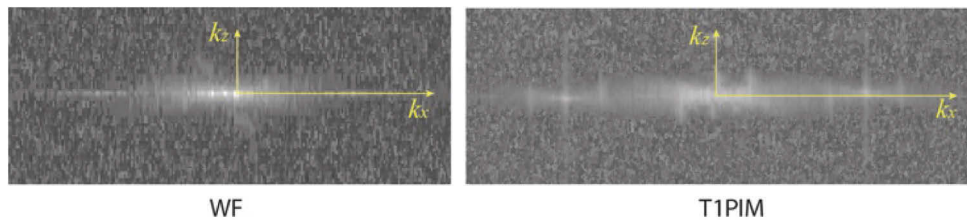


Fig. 11. 3D Fourier transforms the 3D images provided by the conventional microscope (left) and the T1PIM (right).

5. Conclusions

Summarizing, we report here a scanning-microscope scheme, the T1PIM, that provides directly artifact-free, high-resolution images with optical sectioning without the need for any reconstruction algorithm. These features are achieved by the proper combination of patterned illumination and the scanning of the sample. We have validated the method via experimental data and have demonstrated that taking profit from the parallelized procedure the capture speed is comparable with other scanning microscopes. Based on this work, we submitted a patent application [31].

Funding. European Regional Development Fund; Ministerio de Ciencia, Innovación y Universidades (RTI2018-099041-B-I00); Generalitat Valenciana (PROMETEO/2019/048).

Disclosures. The authors declare that there are no conflicts of interest related to this article.

Data availability. Data underlying the results presented in this paper are not publicly available at this time but may be obtained from the authors upon reasonable request.

References

1. T. Wilson and C.J.R Sheppard, "Theory and practice of scanning optical microscopy," Academic Press (London) 1984.
2. S. W. Hell and J. Wichmann, "Breaking the diffraction resolution limit by stimulated emission: stimulated emission-depletion fluorescence microscopy," *Opt. Lett.* **19**(11), 780 (1994).

3. F. Balzarotti, Y. Eilers, K.C. Gwosch, A.H. Gynn, V. Westphal, F.D. Stefani, J. Elf, and S.W. Hell, "Nanometer resolution imaging and tracking of fluorescent molecules with minimal photon fluxes," *Science* **355**(6325), 606–612 (2017).
4. C. J. R. Sheppard, "Super-resolution in confocal imaging," *Optik* **80**, 53–54 (1988).
5. M. Martínez-Corral and G. Saavedra, "The resolution challenge in 3D optical microscopy," *Prog. Opt.* **53**, 1–67 (2009).
6. E. Sánchez-Ortiga, C.J.R Sheppard, G. Saavedra, M. Martínez-Corral, A. Doblas, and A. Calatayud, "Subtractive imaging in confocal scanning microscopy using a CCD camera as a detector," *Opt. Lett.* **37**(7), 1280–1282 (2012).
7. S. Roth, C. J. Sheppard, K. Wicker, and R. Heintzmann, "Optical photon reassignment microscopy (OPRA)," *Opt Nano* **2**(1), 5 (2013).
8. C. J. Sheppard, S. B. Mehta, and R. Heintzmann, "Superresolution by image scanning microscopy using pixel reassignment," *Opt. Lett.* **38**(15), 2889–2892 (2013).
9. C.B. Müller and J. Enderlein, "Image scanning microscopy," *Phys. Rev. Lett.* **104**(19), 198101 (2010).
10. A.G. York, S. H. Parekh, D. Dalle Nogare, R. S. Fischer, K. Temprine, M. Mione, A. B. Chitnis, C. A. Combs, and H. Shroff, "Resolution doubling in live, multicellular organisms via multifocal structured illumination microscopy," *Nat. Methods* **9**(7), 749–754 (2012).
11. A.G. York, P. Chandris, D.D. Nogare, J. Head, P. Wawrzusin, R.S. Fischer, A. Chitnis, and H. Shroff, "Instant super-resolution imaging in live cells and embryos via analog image processing," *Nat. Methods* **10**(11), 1122–1126 (2013).
12. O. Schulz, C. Pieper, M. Clever, J. Pfaff, A. Ruhlandt, R.H. Kehlenbach, F.S. Wouters, J. Grosshans, G. Bunt, and J. Enderlein, "Double resolution with CSD-ISM," *Proc. Natl. Acad. Sci.* **110**(52), 21000–21005 (2013).
13. C.J.R. Sheppard, "Structured illumination microscopy and image scanning microscopy: a review and comparison of imaging properties," *Phil. Trans. R. Soc. A.* **379**(2199), 20200154 (2021).
14. I. J. Cox, C. J. R. Sheppard, and T. Wilson, "Improvement in resolution by nearly confocal microscopy," *Appl. Opt.* **21**(5), 778–781 (1982).
15. W. Lukosz, "Optical systems with resolving powers exceeding the classical limit," *J. Opt. Soc. Am.* **56**(11), 1463–1471 (1966).
16. W. Lukosz, "Optical systems with resolving powers exceeding the classical limit. II," *J. Opt. Soc. Am.* **57**(7), 932–941 (1967).
17. R. Heintzmann and C. Cremer, "Laterally modulated excitation microscopy: improvement of resolution by using a diffraction grating," *Proc. SPIE* **3568**, 185–196 (1999).
18. M. G. L. Gustafsson, "Extended resolution fluorescence microscopy," *Curr. Opin. Struct. Biol.* **9**(5), 627–628 (1999).
19. M. G. L. Gustafsson, "Surpassing the lateral resolution by a factor of two using structured illumination microscopy," *J. Microsc.* **198**(2), 82–87 (2000).
20. G. E. Cragg and P. T. C. So, "Lateral resolution enhancement with standing evanescent waves," *Opt. Lett.* **25**(1), 46–48 (2000).
21. R. Fedosseev, Y. Belyaev, J. Frohn, and A. Stemmer, "Structured light illumination for extended resolution in fluorescence microscopy," *Optics and Lasers in Engineering* **43**(3-5), 403–414 (2005).
22. J. T. Frohn, H. F. Knapp, and A. Stemmer, "Three-dimensional resolution enhancement in fluorescence microscopy by harmonic excitation," *Opt. Lett.* **26**(11), 828–831 (2001).
23. M. G. L. Gustafsson, D. A. Agard, and J. W. Sedat, "Doubling the lateral resolution of wide-field fluorescence microscopy using structured illumination," *Proc. of SPIE* **3919**, 141–150 (2000).
24. M. G. L. Gustafsson, L. Shao, P. M. Carlton, C. J. R. Wang, I. N. Golubovskaya, W. Z. Cande, D. A. Agard, and J. W. Sedat, "Three-Dimensional Resolution Doubling in Wide-Field Fluorescence Microscopy by Structured Illumination," *Biophysical Journal* **94**(12), 4957–4970 (2008).
25. J. Sola-Pikabea, A. Garcia-Rius, G. Saavedra, J. Garcia-Sucerquia, M. Martinez-Corral, and E. Sanchez-Ortiga, "Fast and robust phase-shift estimation in two-dimensional structured illumination microscopy," *PLoS ONE* **14**(8), e0221254 (2019).
26. J. Lu, W. Min, J.A. Conchello, X.S Xie, and J.W. Lichtman, "Super-resolution laser scanning microscopy through spatiotemporal modulation," *Nano Lett.* **9**(11), 3883–3889 (2009).
27. T. Wilson and A. R. Carlini, "Size of the detector in confocal imaging systems," *Opt. Lett.* **12**(4), 227–229 (1987).
28. E Sánchez-Ortiga, M Martínez-Corral, G Saavedra, and J Garcia-Sucerquia, "Enhancing spatial resolution in digital holographic microscopy by biprism structured illumination," *Opt. Lett.* **39**(7), 2086–2089 (2014).
29. H Shabani, A Doblas, G Saavedra, E Sanchez-Ortiga, and C Preza, "Improvement of two-dimensional structured illumination microscopy with an incoherent illumination pattern of tunable frequency," *App. Optics* **57**(7), B92–B101 (2018).
30. C. Doñate-Buendia, R. Torres-Mendieta, A. Pyatenko, E. Falomir, M. Fernández-Alonso, and G. Mínguez-Vega, "Fabrication by Laser Irradiation in a Continuous Flow Jet of Carbon Quantum Dots for Fluorescence Imaging," *ACS Omega* **3**(3), 2735–2742 (2018).
31. E Sánchez-Ortiga, M Martínez-Corral, G Saavedra, and J. Sola-Picabea, "Microscopio óptico por fluorescencia y método para la obtención de Imágenes de microscopía óptica por fluorescencia," Spanish Patent ES2768448-B2 (21 December 2018).